Elastic constants of natural quartz

Paul Heyliger[a)]
Department of Civil Engineering, Colorado State University, Fort Collins, Colorado 80523

Hassel Ledbetter
Los Alamos National Laboratory (E536), Los Alamos, New Mexico 87545

Sudook Kim
Materials Science and Engineering Laboratory, National Institute of Standards and Technology, Boulder, Colorado 80305

(Received 21 December 2002; revised 18 May 2003; accepted 30 May 2003)

The elastic constants of a natural-quartz sphere using resonance-ultrasound spectroscopy (RUS) are measured. The measurements of the near-traction-free vibrational frequencies of the sphere are matched with the predicted frequencies from the dynamic theory of elasticity, with optimized estimates for the elastic constants driving the differences between these sets of frequencies to a minimal value. The present computational model, although based on earlier approaches, is the first application of RUS to trigonal-symmetry spheres. Quartz shows six independent elastic constants, and our estimates of these constants are close to those computed by other means. Except for C_{14}, after a 1% mass-density correction, natural quartz and cultured quartz show the same elastic constants. Natural quartz shows higher internal frictions. © *2003 Acoustical Society of America.*
[DOI: 10.1121/1.1593063]

PACS numbers: 43.20.Hq, 43.20.Ks, 43.35.Cg [RR]

I. INTRODUCTION

Silicon dioxide (SiO_2) in the form of quartz is Earth's most ubiquitous surface mineral. Perhaps the first measurements of quartz's elastic constants originated with Groth,[1] whose 1895 book showed the representation surface of the Young (extension) modulus E_{ii} measured statically. This surface revealed quartz's moderate elastic anisotropy: $E_{33}/E_{11} = 1.31$.

Quartz's complete elastic constants were studied first by Woldemar Voigt, and his static-measurement results appeared in his epochal *Lehrbuch der Kristallphysik* in 1910.[2] Giebe and Scheibe[3] made, perhaps, the first dynamic measurements. Subsequently, quartz's elastic constants were reported in more than 20 studies.[4–6]

Interest in quartz's elastic constants continues for three reasons: First, quartz's elastic constants remain incompletely understood, mainly because quartz is piezoelectric and we lack a good theory for the elastic constants of piezoelectric crystals.[7] Second, quartz occupies a central place in crystal chemistry-physics because of its many polymorphs. We can study these polymorphs, both experimentally and theoretically, through the elastic constants. Third, quartz's device applications exceed one billion per year.[5] Most of these applications use quartz's macroscopic resonance frequencies, which depend mainly on crystal geometry and elastic constants. Elastic constants can be measured accurately (within a few parts in 10^4) and, because of their tensor nature, they provide essential information for preparing crystal cuts with various piezoelectric properties.[8]

Quartz's elastic constants received extensive review, notably by Cady,[4] Brice,[9] James,[10] and, recently, Ballato.[5]

The present study proceeded with two principal objectives: First, measure the complete elastic constants of natural quartz. Second, analyze the macroscopic vibration frequencies of a trigonal-crystal-symmetry sphere.

We used resonance-ultrasound spectroscopy (RUS) to determine these elastic constants. This method was described thoroughly by Migliori and Sarrao,[11] and, although our approach proceeds similarly, the material's trigonal symmetry requires several modifications to existing models.

Applications of RUS to trigonal crystals are rare. Ohno *et al.*[12] considered the case of rectangular parallelepipeds with the trigonal axis perpendicular to one of the faces in the first attempt to determine the elastic constants of trigonal crystals. Ledbetter *et al.*[6] studied the elastic stiffnesses and internal friction of monocrystal cultured quartz for cylindrical geometries. In both of these studies, the general eigenvalue problem that results from the application of the Ritz method to the basic elasticity problem of a solid in traction-free vibration was separated into four symmery groups based on material symmetry and geometrical symmetry. This reduces the size of the initial eigenvalue problem and results in much faster and more accurate frequency calculations. Our approach requires multiple solutions of this eigenvalue problem for a continuously changing elastic-stiffness tensor, and this separation is a critical step. Willis and colleagues[13] used RUS to study the hexagonal–trigonal phase transformation in $LiKSO_4$. Their study provides a good example of applying Landau theory to a second-order or near-second-order phase transition. Quartz's α–β transition at 573 °C provides another example of such a phase transition.

In the following we describe our theoretical model, measurement system, and results of their combination.

a)Electronic mail: prh@engr.colostate.edu

II. THEORETICAL FREQUENCIES

A. Geometry and equations of motion

Our specimen was a natural quartz sphere. The predicted resonance frequencies depend on the sphere radius because our variational method of approximation evaluates terms proportional to elastic stiffness over the volume of the solid. Density ρ appears on the right-hand side of the equations of motion:

$$\sigma_{ij,j}=\rho\ddot{u}_i. \tag{1}$$

Here, σ_{ij} denotes stress and u_i displacement. We do not explicitly solve these equations. Instead, we seek an alternative solution to their weak form.

B. Variational formulation

Hamilton's principle for an elastic medium is given by[14]

$$\delta\int_{t_0}^{t}dt\int_V\left[\frac{1}{2}\rho\dot{u}_j\dot{u}_j-\frac{1}{2}C_{ijkl}\epsilon_{ij}\epsilon_{kl}\right]dV+\int_{t_0}^{t}dt\int_S\overline{t}_k\delta u_k dS=0. \tag{2}$$

Here t denotes time, V and S the volume and surface occupied by and bounding the solid, $\overline{t}_k$ the components of the specified surface tractions, δ the variational operator, the overdot differentiation with respect to time, ϵ_{ij} the components of infinitesimal strain, and C_{ijkl} the components of the fourth-order elastic-stiffness tensor. The general constitutive relation for 32-point-group trigonal symmetry represented in rectangular Cartesian coordinates can be expressed in a contracted form of the stiffness tensor as a six-by-six matrix:

$$\begin{Bmatrix}\sigma_1\\ \sigma_2\\ \sigma_3\\ \sigma_4\\ \sigma_5\\ \sigma_6\end{Bmatrix}=\begin{bmatrix}C_{11}&C_{12}&C_{13}&C_{14}&0&0\\ C_{12}&C_{22}&C_{23}&C_{24}&0&0\\ C_{13}&C_{23}&C_{33}&0&0&0\\ C_{14}&C_{24}&0&C_{44}&0&0\\ 0&0&0&0&C_{55}&C_{56}\\ 0&0&0&0&C_{56}&C_{66}\end{bmatrix}\begin{Bmatrix}\epsilon_1\\ \epsilon_2\\ \epsilon_3\\ \epsilon_4\\ \epsilon_5\\ \epsilon_6\end{Bmatrix}. \tag{3}$$

Here we used the conventional contracted notation ($\sigma_{11}=\sigma_1$, $\sigma_{23}=\sigma_4$, $\epsilon_{11}=\epsilon_1$, $2\epsilon_{23}=\epsilon_4$, $C_{1111}=C_{11}$, $C_{1123}=C_{14}$, and so on), and it is understood that the 1, 2, 3 directions are $x_1=x$, $x_2=y$, and $x_3=z$.

Hamilton's principle in contracted notation becomes

$$\begin{aligned}0=&-\int_0^t\int_V\{\sigma_1\delta\epsilon_1+\sigma_2\delta\epsilon_2+\sigma_3\delta\epsilon_3+\sigma_4\delta\epsilon_4+\sigma_5\delta\epsilon_5\\&+\sigma_6\delta\epsilon_6\}dV\,dt+\frac{1}{2}\delta\int_0^t\int_V\rho(\dot{u}^2+\dot{v}^2+\dot{w}^2)dV\,dt\\&+\int_{t_0}^{t}dt\int_S\overline{t}_k\delta u_k dS.\end{aligned} \tag{4}$$

The surface integral in Eq. (4) is close to zero because the only forces engendered by our measurement system are small point forces at the locations where the pinducers contact the specimen. These forces cause little effect on our results; therefore, we neglect them.

The strain-displacement relations are

$$\epsilon_{ij}=\tfrac{1}{2}(u_{i,j}+u_{j,i}). \tag{5}$$

Our displacement components are expressed in terms of the coordinates $x_1=x$, $x_2=y$, $x_3=z$ with the corresponding displacement components $u_1=u(x,y,z)$, $u_2=v(x,y,z)$, and $u_3=w(x,y,z)$. Substitution of the constitutive and strain-displacement equations into Eq. (4) yields the final weak form of the equations of motion. If we integrate by parts and isolate the volume integral, the resulting Euler equations of this statement yield the equations of motion in Eq. (1). This, however, is not our goal. Instead, we seek the solution to the weak form to solve for the unknown frequencies ω and the mode shapes represented by the functions for u, v, w. This requires an assumed form for the displacements.

C. Ritz approximations

In the Ritz method, we seek approximations to the three displacements using finite linear combinations of the form

$$\begin{aligned}u_1(x_1,x_2,x_3)&=\sum_{i=1}^{n}a_j\Psi_j^1(x_1,x_2,x_3),\\ u_2(x_1,x_2,x_3)&=\sum_{i=1}^{n}b_j\Psi_j^2(x_1,x_2,x_3),\\ u_3(x_1,x_2,x_3)&=\sum_{i=1}^{n}d_j\Psi_j^3(x_1,x_2,x_3).\end{aligned} \tag{6}$$

Here the a, b, and d components are unknown constants, and the functions Ψ are known functions of the spatial coordinates used in the specific formulation. Substituting these equations into the weak form yields the matrix equation

$$\begin{aligned}&\begin{bmatrix}[M^{11}]&[0]&[0]\\ [0]&[M^{22}]&[0]\\ [0]&[0]&[M^{33}]\end{bmatrix}\begin{Bmatrix}\{a\}\\ \{b\}\\ \{c\}\end{Bmatrix}\omega^2\\&+\begin{bmatrix}[K^{11}]&[K^{12}]&[K^{13}]\\ [K^{21}]&[K^{22}]&[K^{23}]\\ [K^{31}]&[K^{32}]&[K^{33}]\end{bmatrix}\begin{Bmatrix}\{a\}\\ \{b\}\\ \{c\}\end{Bmatrix}=\begin{Bmatrix}\{0\}\\ \{0\}\\ \{0\}\end{Bmatrix}.\end{aligned} \tag{7}$$

The element matrices used for each of the formulations are given in the Appendix. The resulting eigenvalue problem is solved using the QR algorithm.[15]

Our choice of approximation function is the same as that of Visscher and colleagues.[16] For each of the three displacement components, the following class of basis functions was selected:

$$\Psi(x,y,z)=x^iy^jz^k. \tag{8}$$

Here x, y, z denote the rectangular-cylindrical-coordinate directions of the cylinder and i, j, and k are integers. The primary advantage of casting the problem in this form is that the integrals required by the weak form are simple to evaluate analytically. For the indices i, j, k, the volume integrals over the sphere given in the Appendix (without the elastic constants) have the form[16]

TABLE I. Classification and description of motion and approximation functions for vibrational modes (from Ohno—Ref. 17), with the modal groups for trigonal symmetry shown as four combinations of two subgroups.

Trigonal subset	Type	Component	Subset x	Subset y	Subset z	Classification
AG	OD	u	O	E	E	Longitudinal vibration
		v	E	O	E	
		w	E	E	O	
	OX	u	O	O	O	Torsion along x axis
		v	E	E	O	
		w	E	O	E	
AU	EX	u	E	E	E	Flexure along x axis
		v	O	O	E	
		w	O	E	O	
	EV	u	E	O	O	Axisymmetric flexure
		v	O	E	O	
		w	O	O	E	
BU	EY	u	O	O	E	Flexure along y axis
		v	E	E	E	
		w	E	O	O	
	EZ	u	O	E	O	Flexure along z axis
		v	E	O	O	
		w	E	E	E	
BG	OY	u	E	E	O	Torsion along y axis
		v	O	O	O	
		w	O	E	E	
	OZ	u	E	O	E	Torsion along z axis
		v	O	E	E	
		w	O	O	O	

$$F(i,j,k)=\left\{1,\frac{\pi}{2}\right\}\frac{R^{i+j+k+3}(i-1)!!(j-1)!!(k-1)!!}{(i+j+k+3)!!}. \tag{9}$$

Here R denotes the sphere radius. This is the $(+++)$ octant of the sphere and is one of eight that must be evaluated for each of the terms in these matrices. The braced term is one if two or three of the integers i, j, k are odd. Otherwise it is $\pi/2$. The remaining seven integrals are similar in form except for the sign, which depends on the evenness or oddness of (i,j,k).

Ohno[17] showed that for a trigonal symmetry parallelepiped it is possible to split the final eigenvalue problem into smaller eigenvalue problems based on the symmetries of the material, specimen geometry, and approximation functions. Heyliger and Johnson[18] extended this approach to a trigonal cylinder, and showed that the modal vibration patterns can be split into six subsets. For the sphere, we use the four subsets defined by Ohno and classify each of the functions in Eq. (8) according to the grouping shown in Table I.

III. MEASUREMENTS

We obtained a sphere of natural Brazilian quartz from a local rock shop. The specimen showed a mass density of 2.6466 g/cm^3, determined from the mass and the volume (diameter=4.4998 cm), 0.7% lower than the x-ray-diffraction mass density of a ''perfect'' quartz crystal: 2.6655 g/cm^3. The quartz showed several randomly oriented 2-μm-diam rutile (TiO_2) fibers varying in length from 0.5 to 3 cm with an average of 2 cm. Because the volume fraction of the fibers is small, we ignored them. Except for the rutile fibers, the specimen showed ''perfect'' optical properties, indicating freedom from macroscopic twins. Also, any significant twinning would appear as irregular apparent C_{ij} values.

Quartz possesses trigonal symmetry, the point group 32, and six independent elastic-stiffness coefficients $(C_{11},C_{12},C_{13},C_{14},C_{33},C_{44})$:

$$[C_{ij}]=\begin{bmatrix} C_{11} & C_{12} & C_{13} & C_{14} & 0 & 0 \\ & C_{11} & C_{13} & -C_{14} & 0 & 0 \\ & & C_{33} & 0 & 0 & 0 \\ & & & C_{44} & 0 & 0 \\ & & & & C_{44} & C_{14} \\ & & & & & \frac{1}{2}(C_{11}-C_{12}) \end{bmatrix}. \tag{10}$$

Quartz possesses a troublesome elastic coefficient $C_{14}=-C_{24}=C_{56}$, which complicates the mathematical analysis for relating macroscopic-vibration resonance frequencies. For quartz, $|C_{14}|$ exceeds C_{12} and C_{13}, and thus must be considered. When we invert Eq. (10) to obtain the elastic-compliance matrix $[S_{ij}]$, we see that the familiar relationship for the Young moduli, $E_{ii}=S_{ii}^{-1}$, fails to result. The E_{ii} depend also on C_{14}. Inversion leads to the further curiosity that $C_{44}\neq S_{44}^{-1}$. By inspection of Eq. (10), we see that $C_{14}=0$ leads to a symmetry increase to hexagonal (transverse-isotropic) and five independent C_{ij}, the symmetry of high-temperature (beta) quartz.

We determined the C_{ij} by using resonance-ultrasound spectroscopy (RUS), which we described previously.[19] Briefly, two 10 MHz PZT transducers hold the sphere specimen at two points. One transducer transmits continuous sinusoidal waves to the specimen, and the other transducer detects the specimen's displacement response. We made measurements at 22 °C in vacuum (1.33 Pa [10^{-3} Torr]). This method's principal advantage is that a single frequency sweep on a single specimen yields the complete elastic-stiffness tensor, both the real part C_{ijkl} and the imaginary part Q_{ijkl}^{-1}.

The resonance frequencies depend on specimen shape, size, mass (or mass density), and elastic-stiffnesses. (For nonspherical specimens, frequencies depend also on crystal orientation.) Each resonance consists of linear combinations of independent elastic-stiffness coefficients. Although not reported here, the complete internal-friction ''tensor'' can be calculated from the half-power width of associated resonance peaks.

We obtained the C_{ij} from the resonance frequencies by using an iterative process that minimizes the differences between measured and calculated resonance frequencies with the given C_{ij}, which take modified values for the next iteration. Because of small differences between the measured and calculated resonance frequencies, the C_{ij} calculations excluded the piezoelectric and dielectric effects, the ''piezoelectric stiffening.''

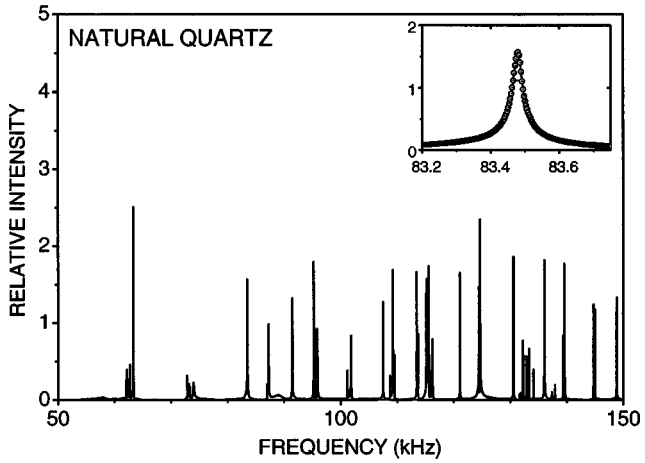

FIG. 1. Resonance spectrum of trigonal-crystal-symmetry, monocrystal quartz sphere. Resonance frequencies give the elastic-stiffness tensor C_{ijkl}. Resonance-peak widths give the imaginary parts of the C_{ijkl}, the internal friction Q^{-1}_{ijkl}.

IV. RESULTS

Figure 1 shows the resonance spectrum. We measured more than 100 resonance frequencies, but selected only the first 45 (30 of which are distinct) for our analysis. Our Ritz model decreases in accuracy with increase in frequency; hence, higher modes are much less accurate than lower modes in our approximation.

The resulting elastic constants are shown in Table II, which also shows our results on cultured quartz, to be re-

TABLE II. Elastic constants and related properties of monocrystal α-quartz.

Property	Natural	Cultured (ordinary)	Cultured (premium)
ρ (g/cm^3)	2.6466±0.01	2.6497±0.0002	2.6497±0.0002
C_{11} (GPa)	87.26	87.16±0.14	87.17±0.05
C_{33} (GPa)	105.8	106.00±0.20	105.80±0.07
C_{44} (GPa)	57.15	58.14±0.08	58.27±0.03
C_{66} (GPa)	40.35	40.26±0.05	40.28±0.02
C_{12} (GPa)	6.57	6.64±0.10	6.610±0.035
C_{13} (GPa)	11.95	12.09±0.21	12.020±0.086
C_{14} (GPa)	−17.18	−18.15±0.08	−18.23±0.03
E_{11} (GPa)	79.41	78.62±0.32	78.61±0.15
E_{33} (GPa)	102.8	102.90±0.23	102.70±0.19
ν_{12}	0.1286	0.1364±0.0059	0.1367±0.0002
ν_{13}	0.0984	0.0985±0.0025	0.0981±0.0008
ν_{31}	0.1274	0.1289±0.0023	0.1282±0.0010
Θ_D (K)[a]	564.0	563.0	563.1
Quasi-isotropic polycrystalline elastic constants obtained by Voigt–Reuss–Hill averaging			
C_l (GPa)	100.2	97.14	100.7
B (GPa)	37.67	37.74	37.69
G (GPa)	46.91	44.55	47.23
E (GPa)	99.45	95.91	99.95
ν	0.0600	0.076 44	0.058 01

[a]Computed numerically from the C_{ij} by averaging the sound velocities from the Christoffel equations' 23 472 directions.

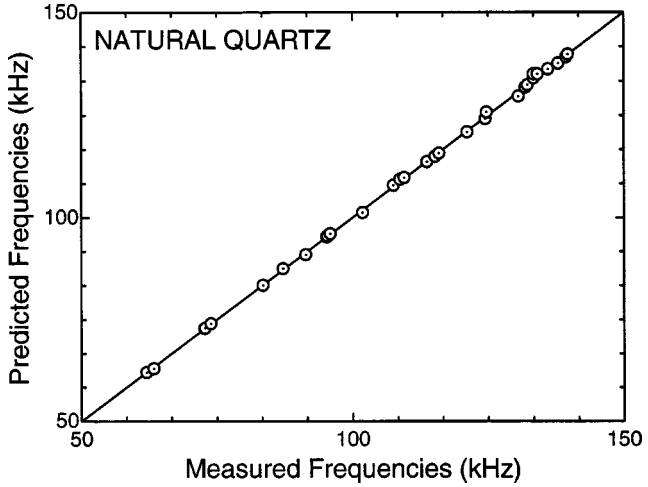

FIG. 2. Predicted versus measured resonance frequencies. Predicted values based on a purely elastic model, neglecting piezoelectric stiffening.

TABLE III. Measured and calculated resonance frequencies (in MHz) for quartz sphere.

Mode	ω_m	ω_c	Diff. (%)	Group
1	0.062 046	0.062 085	0.06	1
2	0.062 046	0.062 085	0.06	4
3	0.063 338	0.062 987	−0.55	2
4	0.063 338	0.062 987	−0.55	3
5	0.072 716	0.072 871	0.21	1
6	0.072 847	0.072 929	0.11	3
7	0.073 886	0.074 004	0.16	1
8	0.073 886	0.074 004	0.16	4
9	0.083 449	0.083 408	−0.05	4
10	0.087 210	0.087 468	0.30	1
11	0.087 210	0.087 468	0.30	4
12	0.091 391	0.090 919	−0.52	3
13	0.091 391	0.090 919	−0.52	2
14	0.095 250	0.095 285	0.04	3
15	0.095 361	0.095 513	0.16	2
16	0.095 908	0.096 041	0.14	4
17	0.101 855	0.101 206	−0.64	3
18	0.101 855	0.101 206	−0.64	2
19	0.107 530	0.107 857	0.30	3
20	0.108 727	0.109 350	0.57	1
21	0.109 526	0.109 801	0.25	2
22	0.109 526	0.109 801	0.25	3
23	0.113 717	0.113 633	−0.07	4
24	0.113 717	0.113 633	−0.07	1
25	0.115 216	0.114 980	−0.21	3
26	0.115 216	0.114 980	−0.21	2
27	0.115 955	0.115 728	−0.20	4
28	0.115 955	0.115 728	−0.20	1
29	0.121 118	0.120 943	−0.14	4
30	0.124 481	0.124 158	−0.26	3
31	0.124 684	0.125 763	0.87	2
32	0.130 591	0.129 580	−0.77	1
33	0.131 800	0.131 770	−0.02	1
34	0.131 800	0.131 770	−0.02	4
35	0.132 240	0.132 335	0.07	2
36	0.132 240	0.132 335	0.07	3
37	0.133 352	0.134 049	0.52	2
38	0.133 352	0.134 988	1.23	3
39	0.134 091	0.134 988	0.67	2
40	0.136 039	0.136 227	0.14	4
41	0.137 910	0.137 576	−0.24	1
42	0.137 910	0.137 576	−0.24	4
43	0.139 353	0.139 167	−0.13	3
44	0.139 687	0.139 777	0.06	2
45	0.139 687	0.139 777	0.06	3

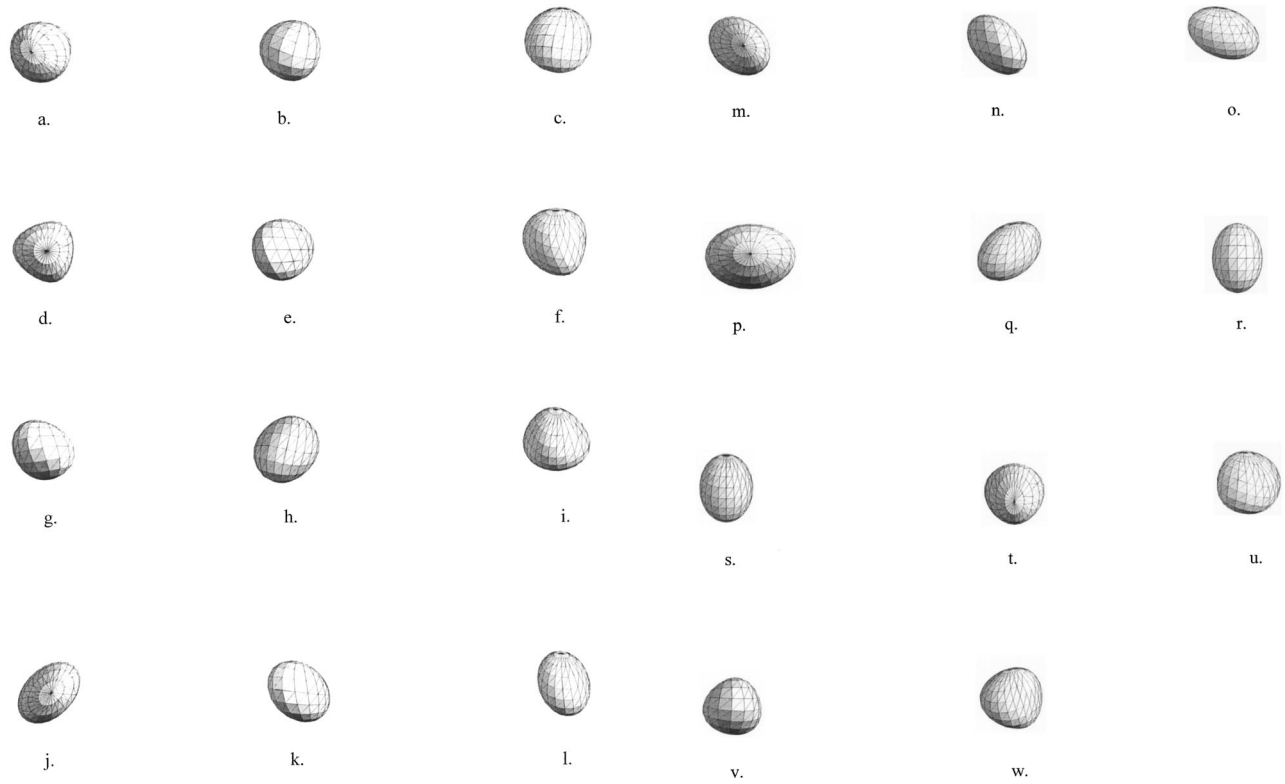

FIG. 3. Deformation diagrams for selected resonances. The three labels for each figure indicate group number, frequency within the group, and the orientation of the viewing perspective. For example, Fig. 1 shows the first mode from group 2 as seen looking toward the origin of the sphere (and coordinate system) along the direction [1,1,1]. (a) 1-1-001, (b) 1-1-010, (c) 1-1-111, (d) 1-2-001, (e) 1-2-010, (f) 1-2-111, (g) 1-3-010, (h) 1-3-100, (i) 1-3-111, (j) 2-1-001, (k) 2-1-010, (l) 2-1-111, (m) 2-2-001, (n) 2-2-010, (o) 2-2-111, (p) 3-1-001, (q) 3-1-111, (r) 3-2-100, (s) 3-2-111, (t) 4-1-001, (u) 4-1-111, (v) 4-2-100, (w) 4-2-111.

ported in detail elsewhere.[6,20] Measurement uncertainties for the natural crystal fall in the same range as those shown for the cultured crystals. Figure 2 shows the relationship between measured and predicted resonance frequencies and provides a basis for neglecting the piezoelectric stiffening. Thus, for quartz, piezoelectric stiffening is relatively small. For other materials, for example, $LiNbO_3$,[21] much larger differences arise between elastic and piezoelectric-dielectric predictions. In piezoelectric crystals, waves propagate with velocities determined by C_{ij}^{E}, E designating constant electric-field intensity, which would be obtained if the crystal were plated with a conductor. Nonplated crystals yield the C_{ij}^{D}, D designating constant electric displacement.

Our fitted frequencies yielded a rms error of 0.36%, slightly higher than typical values for higher-symmetry materials, but still in an acceptable range. Probably, the principal error arises from the specimen's slight nonsphericity. Our fitted frequencies, along with the percentage error and modal group, are shown in Table III. Most frequencies show excellent measurement–model agreement, with only one or two exceptions.

The first ten resonance peaks showed an average internal friction Q^{-1} of 4.7×10^{-4}.

Table II also shows the Debye characteristic temperature Θ_D calculated from the elastic constants.

Figure 3 shows deformation diagrams for selected resonances.

V. DISCUSSION

First, we consider the internal friction Q^{-1}, which arises from various lattice defects. The average Q_{ij}^{-1}, 4.7×10^{-4}, is approximately what we reported for a cultured-quartz crystal with a high dislocation content, $Q^{-1}=1.9\times10^{-4}$,[6] but much higher (by a factor of 34) than the average found for a high-quality (low-dislocation-content), cultured-quartz crystal, 1.4×10^{-5}.[20] Further study of this spherical crystal (strain dependence, frequency dependence, temperature dependence) should identify the source of its higher internal friction. Because of Q^{-1} values as small as 10^{-6} found for other quartz crystals with the same apparatus, we believe the higher Q^{-1} reflects the specimen, not mounting losses.

Second, we consider the natural-quartz versus cultured-quartz elastic constants (Table II). Within measurement errors, no remarkable differences appear. Neglecting C_{14}, the average difference is 0.8%, corresponding closely with the natural crystal's lower mass density and consistent with higher defect content and higher internal friction. Thus, except for a mass-density difference, natural quartz and cultured quartz possess the same elastic constants within a small fraction of 1%, except for C_{14}, where the natural-quartz value is lower by about 5%.

The large specimen-to-specimen variation in C_{14} may result from the lower symmetry of the 32 trigonal point group. When viewed along the c axis, [0001], the crystal structure shows ion shifts away from sixfold symmetry. (See

Fig. 2.32 in Kingery *et al.*[22]) These shifts give rise to the additional elastic stiffness C_{14}. This distorted, or derivative, structure possesses a degree of freedom (the exact ionic positions) that can easily vary among different quartz crystals. Ikeda[20] described C_{14} as the order parameter for the beta–alpha phase transformation. Order-parameter thermodynamics was treated in detail by Landau and Lifshitz.[23]

Our Debye characteristic temperature $\Theta_D = 564\,\mathrm{K}$, calculated as described elsewhere,[24] agrees favorably (but not exactly) with those given by Anderson.[25] $\Theta_D = 545$, 585, 585 K. The spread among the four values ($\pm 3.4\%$) is surprising because if the C_{ij} are measured within 1% (a simple feat), then Θ_D should vary only 0.5%. At zero temperature, the elastic and specific-heat Debye temperatures are theoretically identical.[26] For quartz, Barron and colleagues[27] gave a specific-heat value of $\Theta_D = 558\,\mathrm{K} \pm 6\,\mathrm{K}$. Because Θ_D varies as $G^{1/2}$ (G denotes effective shear modulus), we used the shear modulus to correct our Θ_D to zero temperature, and we obtained $\Theta_D^0\,(\mathrm{elastic}) = 567\,\mathrm{K}$, 1.5% higher than the Barron *et al.* value and 0.5% above their estimated upper bound, 564 K.

VI. CONCLUSIONS

(1) One can solve the problem of macroscopic vibration frequencies of a trigonal-crystal-symmetry sphere. And one can use this analysis to determine the complete elastic-stiffness tensor C_{ijkl} of a material such as quartz.

(2) Natural quartz shows a high internal friction, $Q^{-1} \approx 5 \times 10^{-4}$, but only slightly higher than shown by a poor grade of cultured quartz with moderate dislocation content.

(3) Natural and cultured quartz possess nearly identical C_{ijkl} when corrected about 1% for mass density, except for $C_{1123}\,(C_{14})$, which is about 5% lower in natural quartz. We hypothesize that this difference originates in the extra degree of freedom associated with C_{14}, the effective order parameter for the β–α phase transition.

(4) The elastic Debye temperature agrees with the specific-heat Debye temperature within about 1% when the elastic constants are adjusted to 0 K.

ACKNOWLEDGMENT

Part of this study was completed when P.R.H. was an Alexander von Humboldt research fellow at the University of Stuttgart. He gratefully acknowledges this support.

APPENDIX: COEFFICIENT MATRICES

Rectangular Cartesian Coordinates. The elements of the coefficient matrices are given by

$$K_{ij}^{11} = \int_V \left(C_{11} \frac{\partial \varphi_i^u}{\partial x} \frac{\partial \varphi_j^u}{\partial x} + C_{55} \frac{\partial \varphi_i^u}{\partial z} \frac{\partial \varphi_j^u}{\partial z} + C_{56} \frac{\partial \varphi_i^u}{\partial z} \frac{\partial \varphi_j^u}{\partial y} + C_{56} \frac{\partial \varphi_i^u}{\partial y} \frac{\partial \varphi_j^u}{\partial z} + C_{66} \frac{\partial \varphi_i^u}{\partial y} \frac{\partial \varphi_j^u}{\partial y} \right) dV, \tag{A1}$$

$$K_{ij}^{12} = K_{ji}^{21} = \int_V \left(C_{12} \frac{\partial \varphi_i^u}{\partial x} \frac{\partial \varphi_j^v}{\partial y} + C_{14} \frac{\partial \varphi_i^u}{\partial x} \frac{\partial \varphi_j^v}{\partial z} + C_{56} \frac{\partial \varphi_i^u}{\partial z} \frac{\partial \varphi_j^v}{\partial x} + C_{66} \frac{\partial \varphi_i^u}{\partial y} \frac{\partial \varphi_j^v}{\partial x} \right) dV, \tag{A2}$$

$$K_{ij}^{13} = K_{ji}^{31} = \int_V \left(C_{13} \frac{\partial \varphi_i^u}{\partial x} \frac{\partial \varphi_j^w}{\partial z} + C_{14} \frac{\partial \varphi_i^u}{\partial x} \frac{\partial \varphi_j^w}{\partial y} + C_{55} \frac{\partial \varphi_i^u}{\partial z} \frac{\partial \varphi_j^w}{\partial x} + C_{56} \frac{\partial \varphi_i^u}{\partial y} \frac{\partial \varphi_j^w}{\partial x} \right) dV, \tag{A3}$$

$$K_{ij}^{22} = \int_V \left(C_{22} \frac{\partial \varphi_i^v}{\partial y} \frac{\partial \varphi_j^v}{\partial y} + C_{24} \frac{\partial \varphi_i^v}{\partial y} \frac{\partial \varphi_j^v}{\partial z} + C_{24} \frac{\partial \varphi_i^v}{\partial z} \frac{\partial \varphi_j^v}{\partial y} + C_{44} \frac{\partial \varphi_i^v}{\partial z} \frac{\partial \varphi_j^v}{\partial z} + C_{66} \frac{\partial \varphi_i^v}{\partial x} \frac{\partial \varphi_j^v}{\partial x} \right) dV, \tag{A4}$$

$$K_{ij}^{23} = K_{ji}^{32} = \int_V \left(C_{23} \frac{\partial \varphi_i^v}{\partial y} \frac{\partial \varphi_j^w}{\partial z} + C_{24} \frac{\partial \varphi_i^v}{\partial y} \frac{\partial \varphi_j^w}{\partial y} + C_{44} \frac{\partial \varphi_i^v}{\partial z} \frac{\partial \varphi_j^w}{\partial y} + C_{56} \frac{\partial \varphi_i^v}{\partial x} \frac{\partial \varphi_j^w}{\partial x} \right) dV, \tag{A5}$$

$$K_{ij}^{33} = \int_V \left(C_{33} \frac{\partial \varphi_i^w}{\partial z} \frac{\partial \varphi_j^w}{\partial z} + C_{44} \frac{\partial \varphi_i^w}{\partial y} \frac{\partial \varphi_j^w}{\partial y} + C_{55} \frac{\partial \varphi_i^w}{\partial x} \frac{\partial \varphi_j^w}{\partial x} \right) dV. \tag{A6}$$

[1] P. Groth, *Physicalische Kristallographie und Einleitung in die Kristallographische Kenntniss der Wichtigsten Substanzen* (Oldenbourg, Berlin, 1895).
[2] W. Voigt, *Lehrbuch der Kristallphysik* (Teubner, Leipzig, 1910).
[3] E. Giebe and A. Scheibe, "On the series relationships of the natural elastic frequencies of quartz rods," Ann. Phys. (Leipzig) **9**, 93–175 (1931).
[4] W. Cady, *Piezoelectricity* (McGraw–Hill, New York, 1946).
[5] A. Ballato, "Elastic properties of crystalline quartz," in *Handbook of Elastic Properties of Solids, Liquids, Gases* (Academic, San Diego, 2001), Vol. II, pp. 257–275.
[6] H. Ledbetter, S. Kim, and M. Lei, "Elastic stiffnesses and internal friction of monocrystal quartz" (unpublished).
[7] M. Born and K. Huang, *Dynamic Theory of Crystal Lattices* (Oxford, University Press, London, 1954), especially Secs. 25 and 32.
[8] T. Ikeda, *Fundamentals of Piezoelectricity* (Oxford University Press, Oxford, 1990), 241 pp.
[9] J. Brice, "Crystals for quartz resonators," Rev. Mod. Phys. **57**, 105–146 (1985).
[10] B. James, "Determination of the elastic and dielectric properties of quartz," Ph.D. thesis, University of London, London, 1987.
[11] A. Migliori and J. Sarrao, *Resonant Ultasound Spectroscopy* (Wiley Interscience, New York, 1997).
[12] I. Ohno, S. Yamamoto, O. Anderson, and J. Noda, "Determination of elastic constants of trigonal crystals by the rectangular parallelepiped resonance method," J. Phys. Chem. Solids **12**, 1103–1108 (1986).
[13] F. Willis, R. Leisure, and T. Kanashiro, Phys. Rev. B **54**, 9077–9085 (1996).
[14] H. Tiersten, *Linear Piezoelectric Plate Vibrations* (Plenum, New York, 1969).
[15] L. Mierovitch, *Computational Methods in Structural Dynamics* (Sijthoff & Noordhoff, Alphen aan den Rijn, Netherlands, 1980).
[16] W. Visscher, A. Migliori, T. Bell, and R. Reinert, "On the normal modes of free vibration of inhomogeneous and anisotropic elastic objects," J. Acoust. Soc. Am. **90**, 2154–2162 (1991).
[17] I. Ohno, "Free vibration of a rectangular parallelepiped crystal and its

application to determination of elastic constants of orthorhombic crystals,'' J. Phys. Earth **24**, 355–379 (1976).
[18] P. Heyliger and W. Johnson, ''Traction-free vibrations of finite trigonal elastic cylinders,'' J. Acoust. Soc. Am. **113**, 1812–1825 (2003).
[19] H. Ledbetter, C. Fortunko, and P. Heyliger, ''Orthotropic elastic constants of a boron–aluminum fiber-reinforced composite: An acoustic-resonance-spectroscopy study,'' J. Appl. Phys. **78**, 1542–1546 (1995).
[20] H. Ledbetter and S. Kim, ''Elastic constants and internal frictions of premium cultured quartz'' (unpublished).
[21] H. Ogi, Y. Kawasaki, M. Hirao, and H. Ledbetter, ''Acoustic spectroscopy of lithium niobate: Elastic and piezoelectric coefficients,'' J. Appl. Phys. **92**, 2451–2456 (2002).
[22] W. Kingery, H. Bowan, and D. Uhlmann, *Introduction to Ceramics* (Wiley, New York, 1976), p. 74. Also in Ref. 4, p. 735, Fig. 163.
[23] L. Landau and E. Lifshitz, *Statistical Physics*, Course of Theoretical Physics, Volume 5 (Pergamon, Oxford, 1980), Secs. 142–146.
[24] H. Ledbetter and S. Kim, ''Monocrystal elastic constants and derived properties of the cubic and hexagonal elements,'' in *Handbook of Elastic Properties of Solids, Liquids, and Gases* (Academic, San Diego, 2001), Vol. II, pp. 97–106.
[25] O. Anderson, ''Determination and some uses of isotropic elastic constants of polycrystalline aggregates using single-crystal data,'' Phys. Acoust. **III-B**, 43–95 (1965).
[26] G. Leibfried and W. Ludwig, ''Theory of anharmonic effects in crystals,'' Solid State Phys. **12**, 275–444 (1961).
[27] T. Barron, J. Collins, T. Smith, and G. White, J. Phys. C **15**, 4311–4326 (1980).